Structural study of the electron-doped manganites $Sm_{0.1}Ca_{0.9}MnO_3$ and $Pr_{0.1}Sr_{0.9}MnO_3$: Evidence of phase separation

C. Martin,* A. Maignan, M. Hervieu, and B. Raveau
Laboratoire CRISMAT, UMR 6508, ISMRA, Boulevard du Maréchal Juin, 14050 Caen, France

Z. Jirák
Institute of Physics of ASCR, Cukrovarnická 10, 16253 Prague 6, Czech Republic

M. M. Savosta
Donetsk Institute of Physics & Technics, Rozy Luxembourg 72, 340114 Donetsk, Ukraine

A. Kurbakov and V. Trounov
PNPI Orlova Grove, Gatchina, Leningrad district, 188350, Russia

G. André and F. Bourée
Laboratoire Léon Brillouin, CEA/Saclay, 91191 Gif-sur-Yvette, France
(Received 20 January 2000; revised manuscript received 17 April 2000)

The investigation of two perovskite manganites with the same carrier concentration of 0.1 electron per Mn has been performed using neutron powder diffraction and electron microscopy, and completed with transport and magnetic measurements. For $Sm_{0.1}Ca_{0.9}MnO_3$, whatever the temperature (from 2 to 300 K), a unique crystalline structure (*Pnma* space group) is observed. The magnetic state below $T_N = T_C = 110$ K is phase separated, consisting of ferromagnetic domains of different sizes ranging from small clusters to macroscopic regions, which are embedded in an antiferromagnetic *G*-type matrix. The high conductivity observed in $Sm_{0.1}Ca_{0.9}MnO_3$ at low temperature is established through a percolation of the ferromagnetic domains. At room temperature, the structure of the analogous compound $Pr_{0.1}Sr_{0.9}MnO_3$ is cubic ($Pm3m$ space group). At low temperature ($T < 200$ K), this manganite exhibits a complex microstructure, consisting of an intergrowth of *G* and *C*-type antiferromagnetically ordered layers, both from tetragonal $I4/mcm$ structure, with appreciable lattice distortion. In agreement with the insulating behavior of $Pr_{0.1}Sr_{0.9}MnO_3$ at low temperature, no ferromagnetism is observed.

I. INTRODUCTION

The exploration of the electron doped manganites $Ln_{1-x}Ca_xMnO_3$ has shown the existence of colossal magnetoresistance (CMR) for x values close to 0.85, i.e., for doping level of 0.15 electron per Mn (formally 15% Mn^{3+}), varying with the nature of the Ln cation.[1] The previous neutron diffraction investigation of $Sm_{0.15}Ca_{0.85}MnO_3$ has evidenced, at low temperature, a mixture of *G* and *C*-type antiferromagnetic (AFM) phases associated with *Pnma* and $P2_1/m$ crystalline structures, respectively.[2] In the phase denoted as the *G*-type by Wollan and Koehler[3] (which prototype is $CaMnO_3$), each Mn ion is surrounded by six Mn neighbors whose spins are antiparallel to the given ion. In the *C*-type arrangement, all atoms have two ferro- and four antiferromagnetic nearest neighbors, leading to ferromagnetic (FM) chains which are AFM coupled. The CMR properties of $Sm_{0.15}Ca_{0.85}MnO_3$ have been attributed to the coexistence of both magnetic arrangements and to the closeness of their T_N's which allow a *C* to *G*-type transition by applying a magnetic field of only few teslas.[2]

It is of importance that the *G*-type AFM phase in these electron-doped manganites allows a ferromagnetic (FM) component to develop for some critical doping level of about 5% Mn^{3+}.[1,4–7] This result is in marked contrast with the situation encountered in the hole-doped perovskite manganites. For instance, 16% and 20% of Mn^{4+} in the Mn^{3+} matrix are required to reach a FM metallic state in the $La_{1-x}Sr_xMnO_3$ and $La_{1-x}Ca_xMnO_3$ series[8,9] whereas only 10% of Mn^{3+} in the Mn^{4+} matrix are sufficient to obtain an itinerant behavior, as for $Sm_{0.1}Ca_{0.9}MnO_3$.[5] This absence of symmetry between hole- and electron-doped manganites is also evidenced by the size effect: for a FM Mn^{3+} rich compound, the Curie temperature (T_C) increases with the average *A*-site cationic size ($\langle r_A \rangle$),[10,11] in contrast to the Mn^{4+} rich manganites where small $\langle r_A \rangle$ values favor the FM state.[1] Furthermore, the FM-like behavior of electron-doped samples is original and is rather characterized by a cluster glass signature,[5] the magnetization increases with the electron doping in $CaMnO_3$, reaching an appreciable value of about 1 μ_B per Mn site for 10–12 % Mn^{3+}, instead of the expected $3.1\mu_B$. For higher doping level, the *G*-type phase disappears at the benefit of a *C*-type one. Such particular behavior, for $x \approx 0.90$, has motivated a detailed structural and magnetic study of the $Ln_{0.1}Ca_{0.9}MnO_3$ manganites.

The present paper deals with the structural study versus temperature of the compound $Sm_{0.1}Ca_{0.9}MnO_3$ and, in less extent, of analogous compound $Pr_{0.1}Ca_{0.9}MnO_3$ in connection with their transport and magnetic properties. The results

TABLE I. Summary of structural parameters for $Sm_{0.1}Ca_{0.9}MnO_3$.

(a)

(1) Crystallographic data for $Sm_{0.1}Ca_{0.9}MnO_3$ at room temperature

SG: *Pnma*, $V=210.47$ Å^3

$a=5.3101(1)$ Å

$b=7.4893(1)$ Å

$c=5.2924(1)$ Å

	x	y	z	B(Å^2)
(Ca, Sm)	−0.0339(3)	0.25	0.0066(5)	0.59(2)
Mn	0	0	0.5	0.12(2)
O_1	0.5105(2)	0.25	−0.0669(3)	0.50(2)
O_2	0.2872(1)	−0.0341(1)	0.7123(1)	0.43(1)

$R_p=3.73$, $R_f=2.34$

(2) Selected interatomic distances (in Å) and angles (deg)

Mn-O_1	1.906(1)×2
Mn-O_2	1.911(1)×2
	1.913(1)×2
Mn-O_1-Mn	158.30(4)
Mn-O_2-Mn	157.20(4)

(b)

(1) Crystallographic data and ordered magnetic moments for $Sm_{0.1}Ca_{0.9}MnO_3$ at 10 K

SG: Pnma, $V=209.31$ Å^3

$a=5.3051(1)$ Å

$b=7.4734(1)$ Å

$c=5.2793(1)$ Å

	x	y	z	B(Å^2)
(Ca, Sm)	−0.0365(2)	0.25	0.0059(5)	0.29(2)
Mn	0	0	0.5	0.03(1)
O_1	0.5113(2)	0.25	−0.0678(2)	0.25(1)
O_2	0.2876(1)	−0.0349(1)	0.7115(1)	0.24(1)

$R_p=4.59$, $R_f=1.94$

$m(G)=2.10(1)\mu_B\|z$ Magnetic $R=2.19$

$m(F)=1.17(3)\mu_B\|z$ or y Magnetic $R=4.80$

(2) Selected interatomic distances (in Å) and angles (deg)

Mn-O_1	1.903(1)×2
Mn-O_2	1.909(1)×2
Mn-O_3	1.912(1)×2
Mn-O_1-Mn	158.02(4)
Mn-O_2-Mn	156.68(4)

on $Pr_{0.1}Sr_{0.9}MnO_3$ are also reported, in order to compare the structures of calcium and strontium systems which exhibit very different magnetotransport properties.[12] We show herein that the low temperature phase of $Sm_{0.1}Ca_{0.9}MnO_3$ and $Pr_{0.1}Ca_{0.9}MnO_3$ consists of a *G*-type antiferromagnetic matrix containing ferromagnetic clusters, which coalescence leads to a percolation path and is thus responsible for the metallicity. In contrast, for $Pr_{0.1}Sr_{0.9}MnO_3$, we observe an intergrowth of *G* and *C*-type AFM structures, without ferromagnetism, in agreement with the insulating behavior of this compound at low temperature. The results—structures and properties—are first given for the $Sm_{0.1}Ca_{0.9}MnO_3$ and $Pr_{0.1}Sr_{0.9}MnO_3$ samples separately and then discussed together.

II. EXPERIMENT

The $Sm_{0.1}Ca_{0.9}MnO_3$ sample has been prepared by mixing MnO_2, CaO, and Sm_2O_3 (with isotope Sm^{152}) in stoichiometric proportions. The powders were first heated at 1000 °C with intermediate grindings and then pressed in the form of pellets. They were then sintered at 1500 °C for 12 h in air with a slow cooling down to 800 °C and finally quenched to room temperature.

As previously reported, the synthesis of $Pr_{0.1}Sr_{0.9}MnO_3$ needs more precautions to obtain a single cubiclike perovskite phase, without hexagonal polytype defects.[13] Stoichiometric amounts of Pr_6O_{11}, $SrCO_3$, and MnO_2 were thoroughly mixed and heated in Ar flow at 1000 °C. The powders, pressed in the form of pellets, were then heated at 1500 °C for 12 h, and slowly cooled down to room temperature in Ar flow. These pellets were annealed at 600 °C during 12 h under oxygen pressure ($PO_2=100$ b).

The x-ray data, iodometric titration and the EDS (energy dispersive spectroscopy) analyses attested that the compounds are monophasic, and exhibit homogeneous compositions, close to the nominal ones:

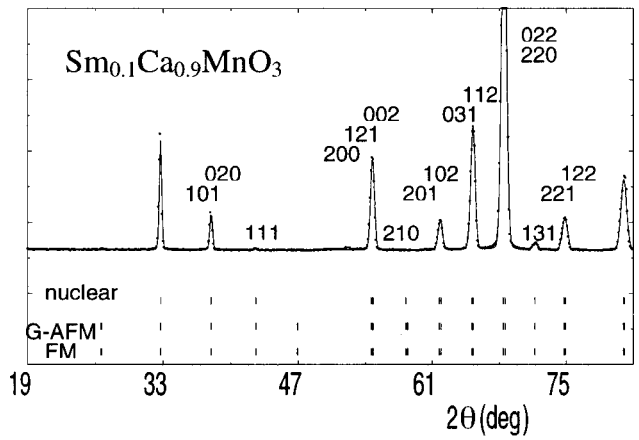

FIG. 1. $Sm_{0.1}Ca_{0.9}MnO_3$ NPD pattern, recorded on the *G*41 diffractometer at 2 K. (The symbols are for the experimental plot and the line for the calculated one. The upper set of Bragg sticks is for the nuclear phase, the middle one for the *G*-type AFM, and the lower one for the FM.)

$Ln_{0.10\pm0.02}(Ca, Sr)_{0.90\pm0.02}MnO_{3.00\pm0.02}$.

Neutron experiments were carried out at LLB (Saclay, France) on the *G*41 diffractometer ($\lambda = 2.4266$ Å) to evidence the structural and magnetic evolution versus temperature. The samples were first cooled and the powder diffraction patterns were recorded, from 2 K to room temperature (RT) by steps of 5 K over an angular range $17 \leqslant 2\theta \leqslant 97°$. Additional patterns using the 3*T*2 diffractometer ($\lambda = 1.227$ Å) were registered in the range $6° \leqslant 2\theta \leqslant 125°$ at 10 K for both samples, at room temperature for the Ca-based compound and at 350 K for the Sr-based one in order to be in the paramagnetic state. The diffraction data were analyzed by using the FULLPROF program.

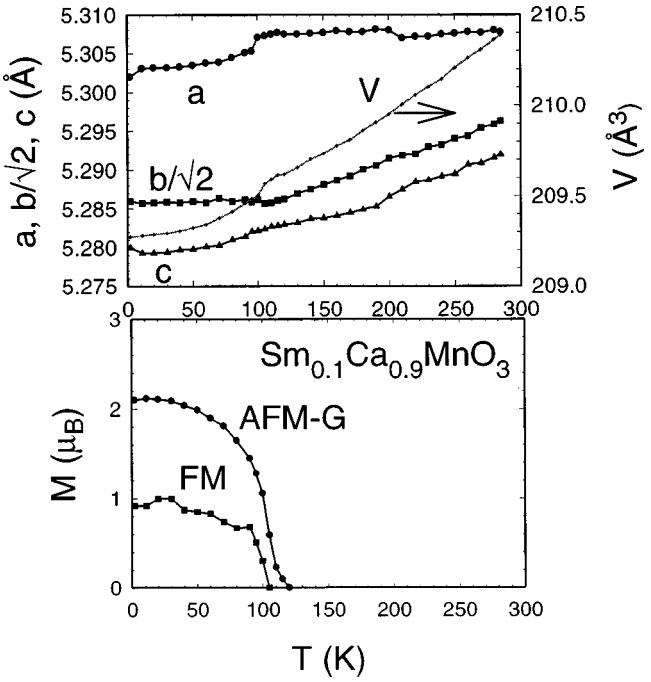

FIG. 2. $Sm_{0.1}Ca_{0.9}MnO_3$; Temperature dependence of the lattice parameters (upper panel, left scale), of the cell volume (upper panel, right scale) and of the average magnetic moments refined for the G-AFM and FM components (lower panel).

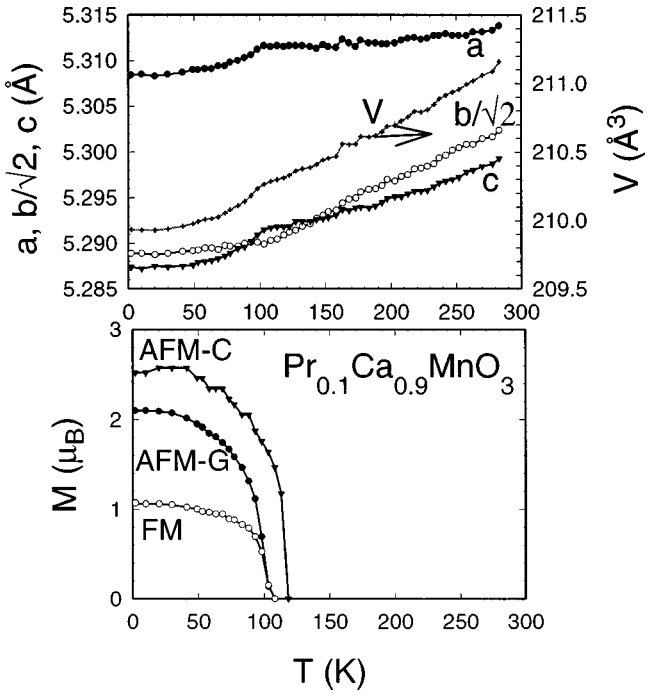

FIG. 3. $Pr_{0.1}Ca_{0.9}MnO_3$: Temperature dependence of the lattice parameters and volume (upper part) and of the G-AFM and FM moments (lower part). The moment in minority *C*-type phase, which is formed below 125 K, is also shown.

The resistivity measurements were performed from room temperature down to 5 K, by the four probe method and the magnetizations were registered on warming with a vibrating sample magnetometer, in 1.4 T applied at 4 K after zero field cooling. The high-temperature susceptibilities were registered with a Faraday balance.

III. RESULTS

A. $Sm_{0.1}Ca_{0.9}MnO_3$

The analysis of the high resolution neutron diffraction patterns recorded at 300 and 10 K leads to the structural parameters summarized in Table I. At room temperature, the

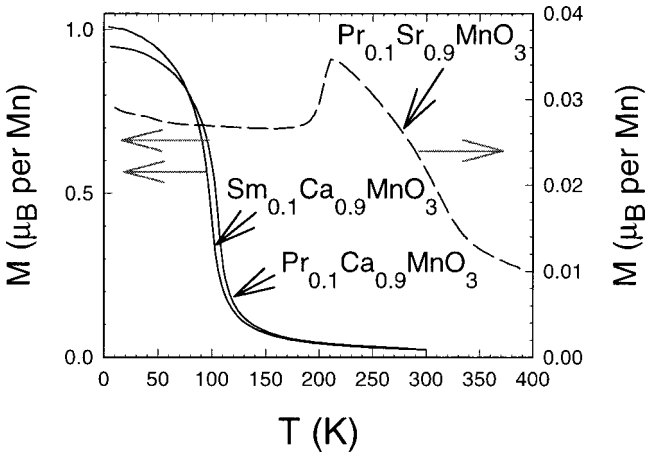

FIG. 4. Temperature dependence of the magnetization for the $Sm_{0.1}Ca_{0.9}MnO_3$, $Pr_{0.1}Ca_{0.9}MnO_3$ and $Pr_{0.1}Sr_{0.9}MnO_3$ samples (1.45 T, zero field cooled).

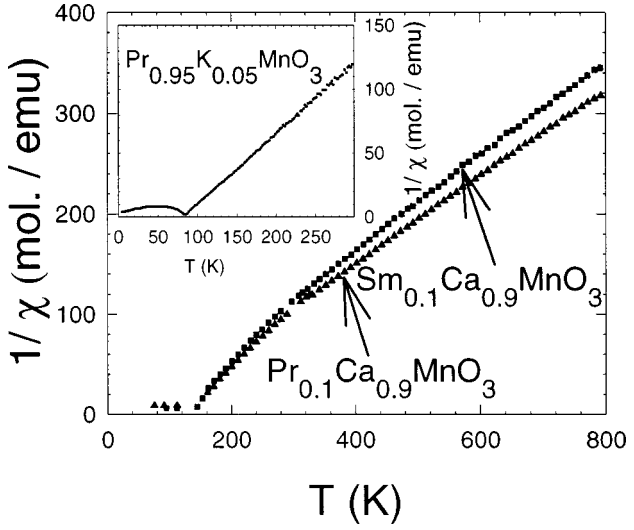

FIG. 5. Inverse susceptibility versus T for $Sm_{0.1}Ca_{0.9}MnO_3$ (squares), $Pr_{0.1}Ca_{0.9}MnO_3$ (triangles), and for $Pr_{0.95}K_{0.05}MnO_3$ in the inset.

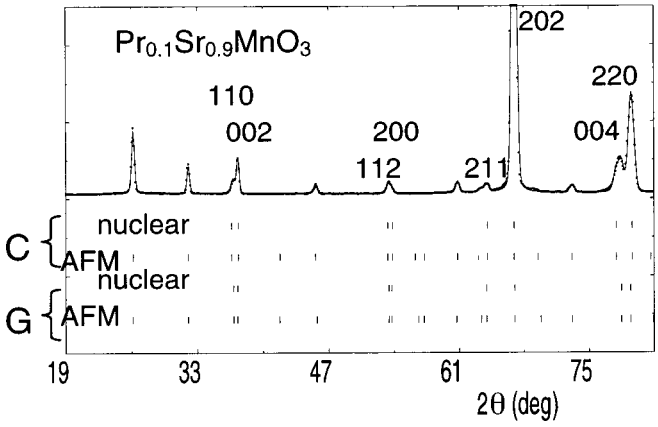

FIG. 6. NPD pattern collected at 2 K for $Pr_{0.1}Sr_{0.9}MnO_3$ (experimental and calculated plots); the Bragg sticks are, from top to bottom, for the C-type phase (nuclear and magnetic lines) and similarly for the G-type one.

$Sm_{0.1}Ca_{0.9}MnO_3$ sample shows the perovskite structure of *Pnma* space group, common for all the $Sm_{1-x}Ca_xMnO_3$ series. The MnO_6 octaedra are nearly regular, with Mn-O distances and Mn-O-Mn tilt angles similar to $Sm_{0.15}Ca_{0.85}MnO_3$. The low-temperature structures are, however, different. The marked monoclinic distortion of $Sm_{0.15}Ca_{0.85}MnO_3$ below 125 K and the magnetic lines associated with the C-type AFM have disappeared. Instead, the $Sm_{0.1}Ca_{0.9}MnO_3$ compound preserves its *Pnma* regular structure and exhibits a particular magnetic order: a mixture of the G-type AFM structure with a FM component (Table I). The temperature dependence of cell parameters and magnetic moments in $Sm_{0.1}Ca_{0.9}MnO_3$ has been determined using the $G41$ patterns (see Fig. 1 for $T=2$ K). The results are reported in Fig. 2. At about 110 K, the FM and AFM components appear simultaneously and only a small decrease is observed on the temperature dependent volume $V(T)$ curve, which in fact corresponds to a decrease of the a and c parameters and an increase of the b one. A similar anisotropic contraction is encountered in the analogous compound $Pr_{0.1}Ca_{0.9}MnO_3$ (Fig. 3). It should be noted that these volume effects are too subtle to be associated with any observable change of distances or tilt angles. Absence of structural transition in the $Sm_{0.1}Ca_{0.9}MnO_3$ sample has been confirmed by the electron diffraction study. Furthermore, the bright field images showed that no twinning phenomena were generated at low temperatures. This behavior excludes the presence of the monoclinic phase, which would be reminiscent of the $Sm_{0.15}Ca_{0.85}MnO_3$ low temperature structure.[2,14]

The magnitudes of the magnetic moment determined from neutron diffraction data on the $Sm_{0.1}Ca_{0.9}MnO_3$ and $Pr_{0.1}Ca_{0.9}MnO_3$ samples are practically identical and they show similar temperature dependencies—more continuous for the $m(G)$ component and more step-like for the $m(F)$ one. The antiferromagnetic moments $m(G)$ are oriented along the shortest orthorhombic *Pnma* axis [001]. The ferromagnetic moment $m(F)$ is oriented either along [001] or [010] axis, but the first case yields a slightly better fit for both compounds. In addition, the $Pr_{0.1}Ca_{0.9}MnO_3$ sample contains 6–7% of the monoclinic C-type phase of the $P2_1/m$ symmetry, with ordered moments oriented along the elongated [1 0 −1] diagonal direction [$m(C)=2.6\mu_B$ per Mn site], in agreement with the previous results on the C-type phase observed in $Sm_{0.15}Ca_{0.85}MnO_3$.[2]

The isothermal magnetization curves $M(H)$, registered with $0 \leqslant H \leqslant 5$ T on $Sm_{0.1}Ca_{0.9}MnO_3$, have already been reported.[5] At 10 K, the magnetization first jumps at $\approx 1\mu_B$ in only 0.5 T but does not saturate in 5 T. More recently, the $M(H)$ data have been collected up to a maximum applied field of 45 T.[15] The magnetization shows only a very weak linear increase in high fields and thus no tendency to achieve 3.1 μ_B per Mn, as expected for fully aligned spins. The temperature dependent magnetization $M(T)$ measured in applied field of 1.45 T (Fig. 4) gives for $Sm_{0.1}Ca_{0.9}MnO_3$ and $Pr_{0.1}Ca_{0.9}MnO_3$ similar ferromagnetic moments of about 1.0 μ_B per Mn; the closeness of this value with the FM moment refined from neutron data will be discussed later. The magnetization vanishes at $T_C=110$ K and a concomitant increase of the electric resistivity is observed, in agreement with the scattering increase [see Fig. 8(a)]. The temperature dependence of the inverse susceptibility $\chi^{-1}(T)$ is also a suitable tool to characterize the magnetic state and thus to complete the neutron diffraction studies. The $\chi^{-1}(T)$ curves of the electron doped $Sm_{0.1}Ca_{0.9}MnO_3$ and $Pr_{0.1}Ca_{0.9}MnO_3$ compounds are displayed in Fig. 5 and compared with the susceptibility of a hole-doped manganite with a comparable carrier concentration, namely the sample $Pr_{0.95}K_{0.05}MnO_3$. This hole doped manganite exhibits a true canted structure as evidenced by reorientation phenomena.[16] The antiferromagnetic component (A-type) achieves $2.64\mu_B$ and the ferromagnetic one $1.05\mu_B$,[17] which are very similar to the determined moments for the $Sm_{0.1}Ca_{0.9}MnO_3$ sample. Though these moments are similar for both electron- and hole-doped manganites, the $\chi^{-1}(T)$ curves strongly differ at low temperature (a curvature and an ideal Curie-Weiss behavior are observed respectively), indicating that the ferromagnetism of the Mn^{4+} rich compounds does not come from a canting.

B. $Pr_{0.1}Sr_{0.9}MnO_3$

The analysis of the high resolution neutron diffraction patterns recorded at 350 and 10 K for $Pr_{0.1}Sr_{0.9}MnO_3$ leads to

TABLE II. Summary of structural parameters for $Pr_{0.1}Sr_{0.9}MnO_3$.

(a)

(1) Crystallographic data for $Pr_{0.1}Sr_{0.9}MnO_3$ at 350 K

SG: $Pm3m$, $V=55.72(222.88)$ Å^3

$a=3.8195(1)$ Å

	x	y	z	B(Å^2)
Pr, Sr	0.5	0.5	0.5	0.50(1)
Mn	0	0	0	0.25(2)
O	0.5	0	0	0.72(1)

$R_p=4.55$, $R_f=2.24$

(2) Interatomic distances (in Å)

Mn-O $1.910(1)\times 6$

(b)

(1) Crystallographic data and ordered magnetic moments for $Pr_{0.1}Sr_{0.9}MnO_3$ at 10 K

SG: $I4/mcm$

	x	y	z	B(Å^2)
Pr, Sr	0.5	0	0.25	0.19(2)
Mn	0	0	0	0.01(3)
O_1	0	0	0.25	0.45(4)
O_2 (*C*-type)	0.2633(4)	0.75633(4)	0	0.41(2)
O_2 (*G*-type)	0.250(3)	0.750(3)	0	0.41(2)

42% *C*-type	$a=5.3605(3)$ Å	$V=221.54$ Å^3
	$c=7.7099(6)$ Å	$m(C)=2.97(7)\mu_b \parallel z$
58% *G*-type	$a=5.3655$ Å	$V=220.99$ Å^3
	$c=7.6763(5)$ Å	$m(G)=1.78(6)\mu_B \perp z$

$R_p=8.02$[a]

C-type $R_f=6.22$

Magnetic $R=8.60$

G-type $R_f=6.39$

Magnetic $R=7.54$

(2) Interatomic distances (in Å)

in *C*-type phase	in *G*-type phase
Mn-O_1 $1.927(1)\times 2$	$1.919(1)\times 2$
Mn-O_2 $1.898(2)\times 4$	$1.897(2)\times 4$

[a]The fit (R_p) can be improved significantly using anisotropic temperature factors.

the structural parameters summarized in Table II. At 350 K, the compound shows a cubic $Pm3m$ perovskite structure. Similarly to the previously studied *C*-type antiferromagnet $Pr_{0.15}Sr_{0.85}MnO_3$,[2] the low temperature structure is tetragonally elongated (space group $I4/mcm$). However, the high resolution data, taken at 10 K, reveal that this sample consists of two crystallographic $I4/mcm$ phases, with slightly different lattice parameters, associated with *C* and *G*-type AFM arrangements. The results in Table II(b) show that the MnO_6 octahedra in the low-temperature *C*-type phase are stretched with Mn-O axial ratio of 1.016. There is a rotation of the octahedra along the crystallographic [001] axis by 3.0°, which leads to the Mn-O-Mn angle in the basal plane of 174.0°. This *c*-axis rotation and MnO_6 distortion are slightly lower than those observed in the *C*-type phase of $Pr_{0.15}Sr_{0.85}MnO_3$. A significant stretching of octahedra appears, due to lattice distortion, also for the *G*-type domains (axial ratio 1.011). The structural refinement does not evidence any significant octahedral rotation. Apparently, the Mn-O-Mn angles in the *G*-type domains are very close to 180°. It should be noted that the fit of $Pr_{0.1}Sr_{0.9}MnO_3$ at 10 K can be improved significantly using the anisotropic temperature factors. They show exceptionally large *z*-components, both for oxygen and cationic sites. Such a situation was not previously encountered in the homogeneous *C*-type system $Pr_{0.15}Sr_{0.85}MnO_3$.

The temperature dependence of lattice parameters, determined from the $G41$ patterns (the 2 K record is given in Fig. 6), reveals a complex behavior of the structural and magnetic transitions in the $Pr_{0.1}Sr_{0.9}MnO_3$ sample (Fig. 7). Essentially, the cubic $Pm3m$ phase is retained down to ≈200 K. Nevertheless, a detailed profile analysis of the patterns evidences a very small amount of a distorted phase with the *C*-type magnetic arrangement, arising just below RT. This may be identified to regions in the sample with larger electron carrier concentration. Namely, the tetragonal distortion, which can be determined with certainty at about 240 K where fraction of the distorted phase achieves 3%, is markedly larger than the distortion at helium temperature and reminds the value observed for the $Pr_{0.15}Sr_{0.85}MnO_3$ compound.[2] The fraction of the *C*-type phase increases slowly with decreasing tem-

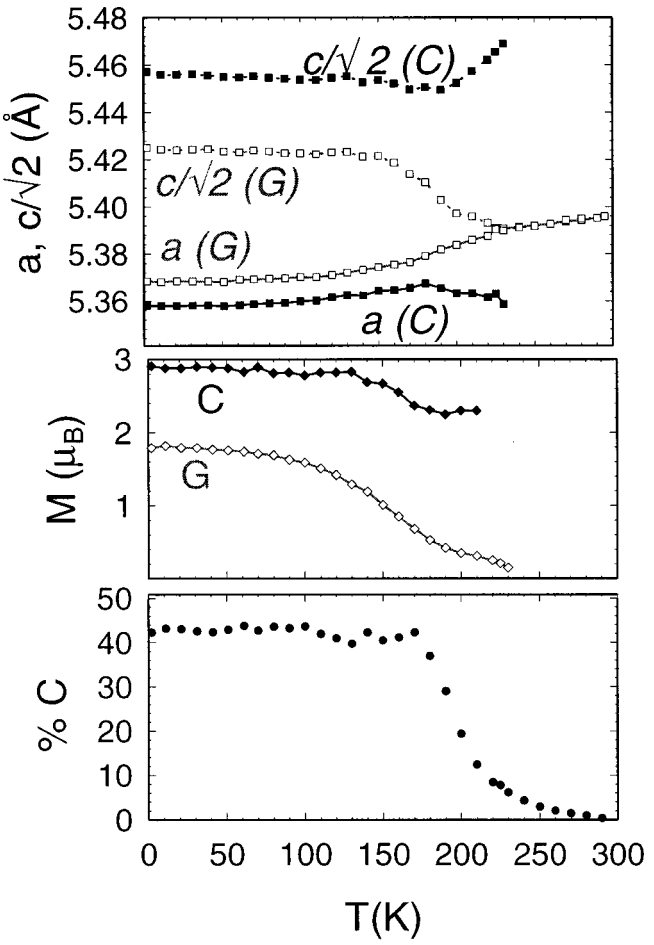

FIG. 7. Temperature dependence of the refined crystallographic parameters of $Pr_{0.1}Sr_{0.9}MnO_3$: Cell parameters (upper panel) and magnetic moments (middle panel) for both phases (coupled with *C* and *G*-type AFM) and ratio of both phases (lower panel).

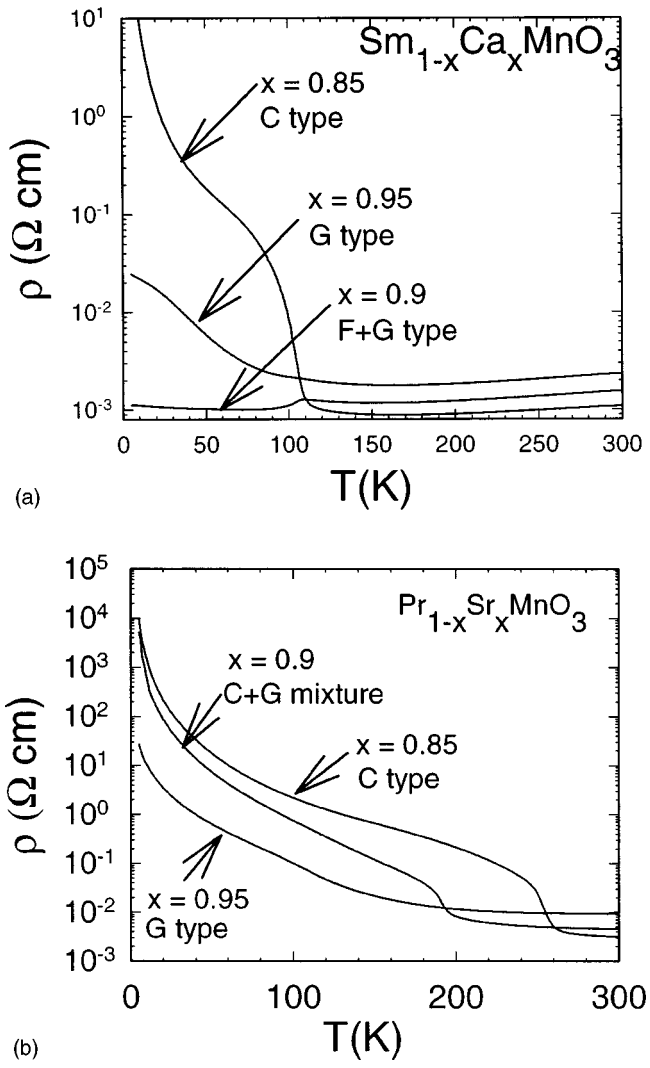

FIG. 8. Resistivity versus temperature for the $Sm_{1-x}Ca_xMnO_3$ (a) and $Pr_{1-x}Sr_xMnO_3$ (b) series. The *x* values are labeled on the graphs.

perature and reaches 8% at 220 K. Below this temperature, a tetragonal distortion develops also in the main cubic phase and, at the same time, the fraction of the minority *C*-type antiferromagnetic phase starts to increase more rapidly and saturates to 42% at about 170 K. The *C*-type ordered moments, 2.97 μ_B at 10 K, are oriented along the tetragonal elongated [001] axis. The *G*-type antiferromagnetic main phase appears in a rather diffuse way, as shown in the $m(G)$ versus T curve in Fig. 7, and the corresponding moments, 1.78 μ_B at 10 K, are perpendicular to the tetragonal [001] axis.

At this stage of the characterization, it is of first importance to determine whether the biphasic magnetic state of $Pr_{0.1}Sr_{0.9}MnO_3$ is due to a cationic segregation. The composition and structural homogeneity of the sample was thus investigated in detail by the EDS technique coupled with electron diffraction by varying the size of the analyzed areas. It is determined that even at the scale of selected areas of a few tens nanometer wide, the Pr/Sr ratio is highly constant and corresponds to the nominal one, in the limit of accuracy of the technique. Thus, the maximum deviation from nominal composition measured on several tens of crystallites is 0.02, i.e., $Pr_{0.10\pm0.02}Sr_{0.90\pm0.02}Mn$. Compared to the analyses usually obtained in such complex oxides, the cationic distribution can be considered as homogeneous. These results show that there is no cationic phase separation at the nanometer scale. Furthermore, the neutron diffraction refinement of the Pr/Sr occupation factors at 350 and 10 K, independently for both crystalline phases at low temperature or together, leads to similar results: the differences observed on this Pr/Sr ratio are within the experimental errors.

The $M(T)$ curve (dashed line in Fig. 4) shows a typical decrease below $T_N \approx 200$ K, as expected for an antiferromagnet. The magnetization of only 0.02 μ_B per Mn, observed at low temperature, excludes the presence of significant ferromagnetic component in the *G*-type domains, in contrast to $Sm_{0.1}Ca_{0.9}MnO_3$. The discrepancy between $Pr_{0.1}Sr_{0.9}MnO_3$ and $Sm_{0.1}Ca_{0.9}MnO_3$ is further manifested in the electronic properties, as shown from the $\rho(T)$ curves of Fig. 8. The resistivity of $Pr_{0.1}Sr_{0.9}MnO_3$ exhibits first a steep increase in the 200 K region, associated with the occurrence of the *C*-type distorted phase, followed with further localization at the lowest temperatures. In this respect, the absence of steep resistivity increase for the less doped manganite $Pr_{0.05}Sr_{0.95}MnO_3$ [Fig. 8(b)] is consistent with a decrease of the *C*-type phase fraction in that compound (16% at 10 K).

TABLE III. Lattice constants (in Å) for $Sm_{0.15}Ca_{0.85}MnO_3$ (from Ref. 2) at 10 and 110 K and $Pr_{0.1}Sr_{0.9}MnO_3$ at 10 K, in doubled cells.

		$Sm_{0.15}Ca_{0.85}MnO_3$ 10 K		$Sm_{0.15}Ca_{0.85}MnO_3$ 110 K		$Pr_{0.1}Sr_{0.9}MnO_3$ 10 K
		7.4547		7.4629		7.5809
C-type	94%	7.4432	64%	7.4499	42%	7.5809
		7.5942		7.5870		7.7099
		($\beta = 90.28°$)		($\beta = 90.28°$)		
		7.5005		7.5023		7.5880
G-type	6%	7.4826	36%	7.4839	58%	7.5880
		7.5005		7.5023		7.6763
		($\beta = 90.30°$)		($\beta = 90.30°$)		

IV. DISCUSSION AND CONCLUDING REMARKS

The present study of electron doped manganites raises two important questions: what is the microscopic nature of the coexistence of the *G*-type antiferromagnetic and ferromagnetic components in the $Ln_{0.1}Ca_{0.9}MnO_3$ systems, and why is ferromagnetism absent in the *G*-type phase of $Pr_{0.1}Sr_{0.9}MnO_3$?

Concerning the latter problem, it is useful to compare the lattice parameters observed at 10 K with previous high resolution neutron diffraction data of $Sm_{0.15}Ca_{0.85}MnO_3$ at 10 K and 110 K,[2] which also exhibit different mixtures of the *G* and *C*-type phases. It is seen in Table III that, irrespective of the *G*-type phase fraction in $Sm_{0.15}Ca_{0.85}MnO_3$, the *G*-type lattice parameters are pseudocubic and incompatible with any parameter of the distorted *C*-type cell. This means that the intergrowth of both phases within one crystal grain is unlikely or otherwise it would involve detectable structural effects. In contrast, the *G* and *C*-type phases in $Pr_{0.1}Sr_{0.9}MnO_3$ show very close *a* parameters, and the unexpected tetragonal distortion of the *G*-type structure strongly suggests that both phases are elastically coupled. Taking into account also the large anisotropy of temperature factors, we conclude that the $Pr_{0.1}Sr_{0.9}MnO_3$ structure should be regarded as an intergrowth of the *G* and *C*-type (0 0 1) layers. This intergrowth could be viewed as a microscopic phase separation, coming from a room temperature homogeneous system.[18] Moreover, the enhancement of the *C*-type volume with a steep increase of the *G*-type ordered moment below ≈200 K (Fig. 5) suggests that some electrons are expelled from the *G*-type regions and that they stabilize the *C*-type ordering in other parts of the sample. In the low temperature *G*-phase of $Pr_{0.1}Sr_{0.9}MnO_3$, both the large local distortions caused by the intergrowth and the electronic separation reduce necessarily the itinerancy of manganese e_g electrons.

Concerning the ferromagnetic component in the *G*-type phase of calcium systems, a homogeneous canted mode of the G_zF_y coupling was proposed in the recent neutron diffraction study of $Ho_{0.1}Ca_{0.9}MnO_3$.[19] On the basis of present high resolution neutron diffraction data on $Sm_{0.1}Ca_{0.9}MnO_3$ and $Pr_{0.1}Ca_{0.9}MnO_3$ and considering new arguments, we suggest an alternative model consisting of an inhomogeneous mixture of antiferromagnetic and ferromagnetic arrangements (the magnetic two-phase model G_z+F_z). The most direct evidence comes from a preliminary NMR (nuclear magnetic resonance) study on $Pr_{1-x}Ca_xMnO_3$ ($x=0.9$, 0.95, and 0.975),[20] which shows indeed a superposition of signals from the majority antiferromagnetic and minority ferromagnetic regions and by the above mentioned shift of the resistivity anomaly with applied magnetic field. This observation suggests that the resistivity drop below $T_N=T_C=110$ K comes from the ferromagnetic regions in the sample. Within the inhomogeneous $G+F$ model, the neutron data should be recalculated with respect to those given in Table I(b) and presented, instead, in terms of volume fractions. The amount of the long range ordered FM domains (reflected in the magnetic diffraction) can be estimated to ≈15%, supposing that the manganese moments reach the theoretical limit of $3.1\,\mu_B$. On the other hand, moments in the *G*-type matrix may be lower, due to the Mn($3d$)-O($2p$) hybridization and cancelling of the spin density on the oxygen site. A value of $2.6\,\mu_B$ is a reliable estimation based on the neutron diffraction data of Wollan and Koehler on $CaMnO_3$.[3] In that case, the antiferromagnetic phase would occupy ≈65% of the sample. The remaining 20% is assumed to be occupied by ferromagnetic clusters not detected by neutron diffraction but which can be easily polarized in a weak external field. In total, about 15% of long-range ordered domains and ≈20% of clusters are responsible for the observed net magnetization of about $1.0\,\mu_B$ at the helium temperature.

The origin of ferromagnetism in the antiferromagnetic *G*-type matrix can be understood considering the early idea of Goodenough[21] that the electron carriers, in low enough concentration, are trapped by potential of trivalent Ln cations. In this framework, the extra electron added by the Ln substitution is shared in a cube of eight Mn^{4+} ions—four of spin up and four of spin down in the ideal *G*-type arrangement. In the dilute limit, such octants ($8\,Mn^{4+}+e^-$) are isolated in the lattice and the electron is localized in a random position with reversal of one Mn^{4+} spin. With increasing doping, the randomly distributed Ln centered octants form clusters in which the extra electrons are no more isolated, giving rise to the electron itinerancy and persistent ferromagnetism according to the double-exchange mechanism. This means that the average size of the metallic ferromagnetic clusters will depend critically on the Ln concentration, i.e., on the electron doping level, in accordance with previous observations.[1,4] For a real knowledge of this local ferromagnetism, a more complex analysis of the NMR spectra of the $Ln_{1-x}Ca_xMnO_3$ manganites in the range $x=0.90-1.0$ is absolutely necessary.

In conclusion, the low temperature state of the electron doped systems with about 10% Mn^{3+}, injected by the Ln^{3+} for Ca^{2+} substitution in $CaMnO_3$, involves ferromagnetic regions in the *G*-type antiferromagnetic matrix. The ferromagnetically ordered spins form regions of various sizes and topologies, from small clusters and dendritic objects to larger 3D regions detected by the neutron diffraction. The high conductivity observed in these *G*-type systems could be established through the coalescence[22] of the larger metallic domains, which content ($\approx$15%) is close to the percolation threshold ($\approx$16%).[18] In the strontium based system $Pr_{0.1}Sr_{0.9}MnO_3$, the AFM ordering appears at temperature well above the T_N of $Sm_{0.1}Ca_{0.9}MnO_3$ and is thus more stable. Moreover, the large distortions of the *G*-type domains imposed by the intergrowth with the *C*-type phase do not allow the charge delocalized ferromagnetic state to develop. Consequently, the absence of ferromagnetism can be ascribed to the particular microstructure of this compound, characterized by large average *A*-site cationic size ($\langle r_A \rangle = 1.297$ Å) and *A*-site cationic size disorder ($\sigma^2 = 1.52 \times 10^{-3}$ Å^2) values.[10,11,23] Finally, although two different magnetic phases (*G*-type antiferromagnetic and ferromagnetic one) have been evidenced in the $Sm_{0.1}Ca_{0.9}MnO_3$ compound a unique crystallographic phase was identified. This is in contrast to $Pr_{0.1}Sr_{0.9}MnO_3$ where the *G* and *C*-type antiferromagnetic arrangements are associated with two crystallographic phases. These electron doped manganites present thus two different examples of the magnetic and electronic phase separations.

ACKNOWLEDGMENT

Two of us (Z.J. and M.S.) acknowledge the financial support of the Grant Agency of the Czech Republic (Grant No. 202/99/0413).

*Corresponding author. FAX: +33 2 31 95 16 00. Email address: christine.martin@ismra.fr

[1] A. Maignan, C. Martin, F. Damay, and B. Raveau, Chem. Mater. **10**, 950 (1998).
[2] C. Martin, A. Maignan, M. Hervieu, B. Raveau, Z. Jirak, A. Kurbakov, V. Trounov, G. André, and F. Bourée, J. Magn. Magn. Mater. **205**, 184 (1999).
[3] E. O. Wollan and W. C. Koehler, Phys. Rev. **100**, 545 (1955).
[4] C. Martin, A. Maignan, F. Damay, M. Hervieu, and B. Raveau, J. Solid State Chem. **134**, 198 (1997).
[5] A. Maignan, C. Martin, F. Damay, B. Raveau, and J. Hejtmanek, Phys. Rev. B **58**, 2758 (1998).
[6] V. A. Bokov, N. A. Grigoryan, and M. F. Bryzhina, Phys. Status Solidi **20**, 745 (1967).
[7] H. Chiba, M. Kikuchi, K. Kusaba, Y. Muraoka, and Y. Syono, Solid State Commun. **99**, 499 (1996).
[8] A. Urushibara, Y. Moritomo, T. Arima, A. Asamitsu, G. Kido, and Y. Tokura, Phys. Rev. B **51**, 14 103 (1995).
[9] P. Schiffer, A. P. Ramirez, W. Bao, and S. W. Cheong, Phys. Rev. Lett. **75**, 3336 (1995).
[10] R. Mahesh, R. Mahendiran, A. K. Raychaudhuri, and C. N. R. Rao, J. Solid State Chem. **114**, 297 (1995); **120**, 204 (1995).
[11] H. Y. Hwang, S. W. Cheong, P. G. Radaelli, M. Marezio, and B. Batlogg, Phys. Rev. Lett. **75**, 914 (1995).
[12] C. Martin, A. Maignan, M. Hervieu, and B. Raveau, Phys. Rev. B **60**, 12 191 (1999).
[13] M. Hervieu, C. Martin, A. Maignan, G. Van Tendeloo, Z. Jirak, J. Hejtmanek, A. Barnabé, D. Thopart, and B. Raveau, Chem. Mater. **12**, 1456 (2000).
[14] M. Hervieu, A. Barnabé, C. Martin, A. Maignan, F. Damay, and B. Raveau, Eur. Phys. J. B **8**, 31 (1999).
[15] M. Respaud (unpublished).
[16] Z. Jirák, J. Hejtmánek, E. Pollert, M. Maryško, M. Dlouhá, and S. Vratislav, J. Appl. Phys. **81**, 5790 (1997).
[17] Z. Jirák, J. Hejtmánek, K. Knížek, and R. Sonntag, J. Solid State Chem. **132**, 98 (1997).
[18] T. Kimura, Y. Tomioka, R. Kumai, Y. Okimoto, and Y. Tokura, Phys. Rev. Lett. **83**, 3940 (1999).
[19] K. Hagdorn, D. Holwein, J. Ihringer, K. Knorr, W. Prandl, H. Ritter, H. Schmid, and Th. Zeiske, Eur. Phys. J. B **11**, 243 (1999).
[20] M. M. Savosta, P. Novák, M. Maryško, Z. Jirák, J. Hejtmánek, J. Englich, J. Kohout, C. Martin, and B. Raveau (unpublished).
[21] J. B. Goodenough, Phys. Rev. **100**, 564 (1955).
[22] D. Casa, V. Kiryukhin, O. A. Saleh, B. Keimer, J. P. Hill, Y. Tomioka, and Y. Tokura, Europhys. Lett. **47**, 90 (1999).
[23] L. M. Rodriguez-Martinez and J. P. Attfield, Phys. Rev. B **54**, 15 622 (1996).